

An Updated Parametrization of Algorithms to Retrieve the Diffuse Attenuation of Light in the Ocean from Remote Sensing and its Impact on Estimates of Net Primary Productivity

Charlotte Begouen Demeaux^{1*}, Emmanuel Boss¹, and Toby K. Westberry²

¹School of Marine Sciences, University of Maine, 360 Aubert Hall, Orono, ME 04469, USA.

²Department of Botany and Plant Pathology, Oregon State University, Corvallis, OR, 97331, USA.

*Corresponding author: charlotte.begouen@maine.edu

This is a non-peer reviewed preprint submitted to earthArXiv. This manuscript has been submitted for publication in Journal of Remote Sensing. Subsequent versions of this manuscript may have slightly different content. If accepted, the final version of this manuscript will be available via the 'Peer-reviewed Publication DOI' link on the right-hand side of this webpage. Please feel free to contact any of the authors.

1 An Updated Parametrization of Algorithms to Retrieve the
2 Diffuse Attenuation of Light in the Ocean from Remote
3 Sensing and its Impact on Estimates of Net Primary
4 Productivity

5 Charlotte Begouen Demeaux^{1*}, Emmanuel Boss¹, and Toby K. Westberry²

6 ¹School of Marine Sciences, University of Maine, 360 Aubert Hall, Orono, ME
7 04469, USA.

8 ²Department of Botany and Plant Pathology, Oregon State University, Corvallis,
9 OR, 97331, USA.

10 *Corresponding author : charlotte.begouen@maine.edu

11 February 9, 2023

12 **Abstract**

13 We recently found a significant bias while validating frequently used ocean color algorithms
14 retrieving the spectral diffuse attenuation coefficient ($K_d(\lambda)$) and the attenuation coefficient for
15 photosynthetically available radiation ($K_d(PAR)$) [\[1\]](#). Here we compute new coefficients for
16 existing algorithms for $K_d(\lambda)$, so as to remove the observed bias at $K_d(490)$, and evaluate the
17 impact on global and regional estimates of net primary production (NPP) using two different
18 primary production models. The new parametrization results in improved retrieval of $K_d(490)$
19 by both the empirical and the semi-analytical algorithms. Match-ups between BGC-Argo floats
20 and Remote Sensing Reflectance (R_{rs}) for six different satellite sensors no longer have a small-
21 value bias, and show a reduced RMSE and error ratio. The new coefficients are validated using
22 measurements not included in the training dataset and are found to perform significantly better
23 at a different wavelength (412nm) than the one used for the new parametrization (490nm) and
24 perform reasonably well in Case-2 waters. Since the new coefficients presented here were devel-
25 oped with a dataset encompassing a larger proportion of the ocean’s variability, they are better
26 suited to compute $K_d(\lambda)$ in regions that were not present in the original algorithm’s dataset
27 and are therefore appropriate for global $K_d(\lambda)$ estimation. Using the new K_d parameterization
28 results in a global increase of NPP of $\approx 37\%$ in both models used, mostly driven by the previous
29 overestimation of $K_d(\lambda)$ (underestimation of light penetration) in the clear, subtropical gyres.
30 Subtropical gyres show the largest increase (79%) in the VGPM model, with the presence of
31 a strong seasonal cycle in the difference. High $K_d(\lambda)$ areas are less affected by the new pa-
32 rameterization (no increase in NPP in VGPM, $\approx 20\%$ in CbPMv2). Although the subtropical

gyres are not very productive regions of the ocean, their large surface area and the magnitude of the bias in $K_d(\lambda)$ between the old and new parameterization causes the observed significant difference in global NPP estimates. Our results suggest that the oceanic carbon uptake is larger than previously thought, which will be most relevant to the oceanic carbon dioxide budget once humanity slows the increase of atmospheric CO_2 .

1 Introduction

Accurately retrieving the spectral diffuse attenuation coefficient of downwelling irradiance ($K_d(\lambda)$) from Remote Sensing Reflectance (R_{rs}) estimated with Ocean Color radiometry measured on board satellites is of importance when trying to quantify the penetration of solar radiation from the surface to depth. Diffuse attenuation coefficients (K_d s) are Apparent Optical Properties (AOPs) that convey information on the optical properties of the water while being moderately affected by external environmental conditions impacting the light field (such as solar angle, clouds, passing waves and more) [2]. As such, $K_d(\lambda)$ constrains bio-physical processes such as heating, carbon fluxes, photochemistry and is used as an input in many physical or assimilative biogeochemical models [3] as well as primary production models [4].

Because K_d varies as a function of the Inherent Optical Properties (IOPs) of a water body (mostly absorption (a) and back-scattering (b_b), [5]), many algorithms were developed to retrieve K_d from R_{rs} , either through explicit empirical fits to in-situ data (Standard level-2/level-3 product from NASA/ESA [6, 7]), development of implicit neural-network (NN) based algorithms [8], or using semi-analytical algorithms that first retrieve IOPs and then use them to compute K_d [9, 10]. These algorithms were all tuned to data from either Case-1 and/or Case-2 waters and share a common characteristic: they were constrained and validated with a small number of in-situ data points that are not representative of the global ocean, or with radiative-transfer model runs using a range of input data assumed to represent the global ocean, but whose distribution does not match the spatial distribution of optical properties in the ocean. In a previous study [1], building on previous work [11], we compiled a novel global database of radiometry data at three different wavelengths and for PAR obtained with sensors onboard BGC-Argo profiling floats and matched them to coincident observations from six different satellite sensors (MODIS-Aqua, MODIS-Terra, VIIRS-SNPP, VIIRS-JPSS, OLCI-S3A, OLCI-S3B). Results showed a strong bias in the clearest ocean waters for all three evaluated algorithms (empirical, NN, and semi-empirical) with R_{rs} -derived $K_d(\lambda)$ and $K_d(PAR)$ consistently over-estimated, resulting in an underestimation of the depth to which light penetrates. This persistent bias was attributed to the fact that the in-situ data-sets used to validate the algorithms lacked sufficient observations representing the clearest waters of the global ocean where extremely low K_d values are found.

Since the clearest waters of the world represent a significant portion of the surface area of the global ocean, the goal of this current study is to recompute coefficients of an empirical $K_d(490)$ algorithms and a $K_d(\lambda)$ algorithm using the more globally representative BGC-Argo-float database ranging from very clear oligotrophic waters to Case-2 coastal waters. As these data do not represent all ocean regions equally, we take into account the number of data points collected and their distri-

72 bution within and across different biogeochemical regions in the recomputation of the coefficients.
73 We then quantify the impact of the revised parametrization of the attenuation coefficient (K_d) from
74 one algorithm on the estimation of Net Primary Productivity (NPP) using three different net pri-
75 mary production algorithms. We find all NPP models to exhibit a significant difference at the global
76 scale when using the new parametrization of the K_d algorithm. Since NPP represents an essential
77 mechanism for sequestering carbon dioxide from the atmosphere into the ocean, earth-system carbon
78 budgets will likely need to be re-adjusted for the detected bias. We have elected to stay away from
79 $K_d(PAR)$ algorithms (7, 12) as those depend on the depth where we want the product at, and as
80 one can get an accurate estimate of those from $K_d(\lambda)$ as recently validated with data from profiling
81 float (e.g. 11, 13).

82 2 Methods

83 2.1 Float match-up data-set

84 We use the same match-up data-set compiled in our previous study 1 available on the Zenodo
85 repository 1. It contains match-ups of K_d between six different contemporary ocean color satellite
86 sensors and BGC-Argo floats measuring radiometry. Match-up criteria are based on previously
87 published protocols 14.

88 2.1.1 $K_d(\lambda)$

89 The details of the method behind the match-up between BGC-Argo float radiometry and satellite
90 R_{rs} are available in 1. In brief, float-retrieved K_d (herein $K_d^{float}(\lambda)$) is calculated from downwelling
91 irradiance ($E_d(\lambda)$) using an iterative least-squares regression of $E_d(\lambda)$ with depth. This method is
92 preferred to the standard method of extrapolating E_d to the surface to obtain $E_d(\lambda, 0^-)$ and linearly
93 regressing $E_d(\lambda)$ with depth as it avoids introducing bias through the extrapolation. Different
94 techniques for K_d retrieval were evaluated and showed no significant difference in the fidelity of
95 the retrieval 1. Before retrieving $K_d^{float}(\lambda)$, all $E_d(\lambda)$ profiles were quality controlled following
96 a published protocol 15 which removed effects of passing clouds, wave focusing, and other bias-
97 inducing effects.

98 2.2 Regional biome-based weighting and statistical metrics

99 Float coverage and satellite match-ups in the global ocean are unevenly distributed with a substantial
100 proportion of the floats ($\approx 70\%$) in the Western Mediterranean, Eastern Mediterranean and the
101 Southern Ocean (Table 1). Given that the goal of this study is to recompute the algorithms for the
102 global ocean, it is important not to create an additional source of bias by over-fitting the coefficients
103 towards specific regions.

104 In order to perform this biome-weighting, two parameters need to be taken into account 1)
105 the surface area of each biome ($Area_i$) - available from 16 for biomes 1:17 and computed for the

¹<https://www.zenodo.org/record/7015427#.Y5cv30zMJ-U>

106 Mediterranean biomes (Table 1) and 2) the number of match-ups in each biome ($N(Area_i)$) - from
107 the float match-up database. An individual weight (W_i) for each specific match-up can then be
108 computed following:

$$W_i = \frac{Area_i}{N(Area_i)} \quad (1)$$

109 Weights for each region are listed in Table 1. Biomes 2 (North Pacific Subtropical Seasonally
110 Stratified) and 17 (Southern Ocean Ice) have less than 15 match-ups (3 and 2 respectively) across all
111 sensors and are therefore not considered in the rest of this study as their very high individual weight
112 would bias the computation of the new coefficients and because they likely have high uncertainties
113 relative to the central tendency in their own region. They are therefore assigned a N/A weight
114 (Table 1).

115 In order to ensure that the updated algorithms are representative of the global ocean, we used a
116 Monte-Carlo type sub-setting according to the following method: For each sensor, the total number
117 of match-ups in each biome was computed. Within each biome, a certain number of match-ups
118 were extracted in order to obtain a subset that was representative of the percentage of the ocean
119 covered by each biome. The number of match-ups selected in each biome was based on the largest
120 possible amount of match-ups in the biome that had the largest discrepancy between the proportional
121 surface area and the number of actual match-ups. For example, in the case of MODIS-Terra and
122 $K_d(490)$, Biome 4 had the largest discrepancy with only 17 match-ups and a coverage of 12.29% of
123 the ocean. Therefore we selected all 17 match-ups and sub-sampled the other biomes in accordance
124 with the proportional surface area listed in Table 1, for a total number of 135 match-ups. This was
125 repeated 100 times (each time picking random match-ups from each biome), in order to compile a
126 "proportional dataset" for each sensor that was proportionally representative of the global dataset.
127 Statistical metrics were computed over the total proportional dataset for each sensor.

128 Statistical metrics on the whole (unweighted) dataset, not taking into account uneven coverage,
129 are found in the Supplementary material for comparison purposes (Table S1).

Table 1: Area and proportion of the global ocean represented by each Oceanic biome based on [16] and with the two Mediterranean biomes added. The total number of match-ups for the full data-set is reported (with all sensors combined), and the individual weight for each float-Satellite match-up is reported based on the number of match-ups in one specific biome, as well as its relative area as described in equation [1]. Biomes 1,2,3,5 and 17 have less than 15 match-ups and were therefore considered "empty" for the rest of this study, so as not to skew the fitting coefficient of the new parametrization for attenuation algorithms.

Biome Name	Biome Number	Area (10^6 km^2)	Proportion of total area (%)	Number of match-ups	Individual weight of match-ups
North Pacific Ice	1	4.59	1.37	0	N/A
North Pacific Subpolar Seasonally Stratified	2	12.84	3.85	3	N/A
North Pacific Subtropical Seasonally Stratified	3	6.83	2.04	0	N/A
North Pacific Subtropical Permanently Stratified	4	41.05	12.29	170	0.072
West pacific Equatorial	5	11.69	3.50	0	N/A
East Pacific Equatorial	6	14.89	4.46	102	0.044
South Pacific Subtropical Permanently Stratified	7	52.71	15.79	434	0.036
North Atlantic Ice	8	5.48	1.64	225	0.007
North Atlantic Subpolar Seasonally Stratified	9	10.06	3.01	690	0.004
North Atlantic Subtropical Seasonally Stratified	10	5.97	1.79	22	0.081
North Atlantic Subtropical Permanently Stratified	11	17.46	5.23	436	0.012
Atlantic Equatorial	12	7.41	2.22	23	0.097
South Atlantic Subtropical Permanently Stratified	13	18.06	5.41	704	0.008
Indian Ocean Subtropical Permanently Stratified	14	35.94	10.76	16	0.673
Southern Ocean Subtropical Seasonally Stratified	15	29.69	8.89	380	0.023
Southern Ocean Subpolar Seasonally Stratified	16	39.63	11.87	305	0.039
Southern Ocean Ice	17	18.68	5.59	2	N/A
Western Mediterranean	18	0.73	0.22	2493	8.8×10^{-5}
Eastern Mediterranean	19	1.86	0.56	2969	1.9×10^{-4}

2.3 Updated algorithms for R_{rs} -retrieval of $K_d(\lambda)$

2.3.1 Empirical algorithms used for the operational products.

Two different algorithms computing $K_d(490)$ evaluated in [1] and their associated coefficients are here re-parameterized. The first is the operational level-2 and level-3 product for $K_d(490)$ of both NASA and ESA. Although two distinct products, both are based on the same empirically-derived link between in-situ $K_d(490)$ measurements and blue-to-green R_{rs} band ratio [6], originally developed for CZCS with "blue" defined as the wavelength closest to $490nm$ and "green" the sensor's wavelength between $547nm$ and $565nm$. NASA's version² is computed as follows, with the A_i coefficients tuned to each specific sensor, and $K_w(490) = 0.0166 \text{ m}^{-1}$ being the value used for the diffuse attenuation

²https://oceancolor.gsfc.nasa.gov/atbd/kd_490/

139 at 490nm due to seawater.

$$K_d(490)^{NASA} = K_w(490) + 10^{A_0 + \sum_{i=1}^4 A_i \left(\log_{10} \left(\frac{R_{rs}(\lambda_{blue})}{R_{rs}(\lambda_{green})} \right) \right)^i} \quad (2)$$

140 ESA’s version also uses $K_w(490)$, five A_i coefficients, and a blue-to-green reflectance ratio based on
141 [7](#).

$$K_d(490)^{ESA} = K_w(490) + 10^{\sum_{i=0}^4 A_i \left(\log_{10} \left(\frac{R_{rs}(490)}{R_{rs}(560)} \right) \right)^i} \quad (3)$$

142 For the sake of comparison, NASA’s and ESA’s empirical products (applied to their respective
143 sensors) will be grouped together in the statistical metrics and referred to as $K_d(490)^{NASA/ESA}$.

144 2.3.2 Semi-Analytical algorithm based on IOP retrieval.

145 $K_d(\lambda)$ retrieval from the semi-analytical algorithm (herein $K_d(\lambda)^{QAA}$) was first published in 2005 [9](#)
146 and refined in 2013 [10](#). It is based on the relationship between $K_d(\lambda)$, IOPs, and the solar zenith
147 angle (θ). It was constrained using Hydrolight simulations using the synthetic IOCCG data-set [17](#).
148 The IOPs for absorption ($a(\lambda)$) and backscattering ($b_b(\lambda)$) at any wavelength are retrieved from
149 $R_{rs}(\lambda)$ using the Quasi-analytical algorithm (QAA) [18](#) version 6 [3](#) with $\eta_w(\lambda) = b_{b_w}(\lambda)/b_b(\lambda)$:

$$K_d^{QAA}(\lambda) = (1 + 0.005\theta) \times a(\lambda) + (1 - A_1 \times \eta_w(\lambda)) \times A_2 \times (1 - A_3 \times e^{-A_4 \times a(\lambda)}) \times b_b(\lambda). \quad (4)$$

150 Pure water absorption values are retrieved from [19](#) and pure water backscattering is corrected for
151 the effect of salinity following [20](#). Here we recompute the value of the A_i coefficients based on the
152 match-ups at 490nm and keep the coefficient relating to the sun angle (0.005 in equation [4](#)). For
153 other wavelengths the coefficients should be the same (as in Lee’s paper [10](#)).

154 2.4 Independent validation data-sets

155 Recomputed $K_d(\lambda)$ s ($K_d(\lambda)_{NewCoeffs}^{R_{rs}}$) were independently evaluated with existing in-situ and syn-
156 thetic data-sets commonly used in global K_d algorithms development. The NOMAD (NASA bio-
157 Optical Marine Algorithm Data set) data-set [21](#) is an in-situ data-set spanning oligotrophic to
158 eutrophic waters and has been used to develop the operational empirical R_{rs} -retrieved $K_d(490)$
159 level-2/level-3 product from NASA [4](#) and contains about 800 simultaneous $E_d(\lambda)$ and $R_{rs}(\lambda)$ mea-
160 surements. The COASTLOOC data-set consists of oligotrophic to eutrophic measurements in Euro-
161 pean waters and contains 195 pairs of reflectance below the surface ($R(0^-, \lambda)$) and $K_d(\lambda)$. $R(0^-, \lambda)$
162 was converted to R_{rs} with $R_{rs} = 0.133 \times R(0^-, \lambda)$ following [22](#). The International Ocean Color
163 Coordinating Group (IOCCG)’s synthetic data-set, originally designed to develop and validate in-
164 version algorithms [2](#), [17](#) was also used, where data points simulate natural variability over a wide
165 range of Case-1 and Case-2 waters. One thousand paired $R_{rs}(\lambda)$, $K_d(\lambda)$ and associated IOPs such
166 as $a(\lambda)$ and $b_b(\lambda)$ are available from this dataset. All three of these data-sets are independent and
167 have varying ranges different from the newly-compiled float database [1](#). Therefore, they should be

³https://www.ioccg.org/groups/Software_OCA/QAA_v6_2014209.pdf,

⁴<https://seabass.gsfc.nasa.gov/wiki/NOMAD>

168 able to assess the robustness of the new coefficients across a different dynamic range than they were
 169 derived with (higher percentage of high values, strong bias towards specific biomes).

170 Since coefficients for the $K_d^{QAA}(490)$ algorithm are recomputed using $K_d(490)^{float}$, applying the
 171 same coefficients to assess the accuracy of retrieval at another wavelength (such as 412nm to retrieve
 172 $K_d(412)$) provides an additional independent validation for the performance of the new formulation.

173 2.5 Cost functions used for each algorithm

174 New coefficients were computed for the two $K_d(\lambda)^{Rrs}$ and the $K_d(PAR)^{Rrs}$ algorithms by minimizing
 175 the following cost function:

$$\bar{\chi} = \sum_{i=0}^{N(match-ups)} W_i * \frac{|K_d(\lambda, i)_{NewCoeffs}^{Rrs} - K_d(\lambda, i)^{float}|}{Uncertainty_i} \quad (5)$$

176 where W_i is the individual biome-weight of each match-up (see equation 1), $Uncertainty_i$ for
 177 a given match-up defined as the maximum value between a minimum constant uncertainty (0.005)
 178 due to sensor specificity and a percentage (10%) of $K_d(\lambda)^{Rrs}$: $Uncertainty_i = max(0.005m^{-1}, 0.1 * K_d(\lambda)^{Rrs})$
 179 and $K_d(\lambda)_{NewCoeffs}^{Rrs}$ is derived from equations 2, 3, and 4 depending on the algorithm
 180 evaluated. The set of coefficients $A_i, i = 1 : 5$ resulting in the smallest cost function $\bar{\chi}$ is considered
 181 as resulting in the best retrieval for our data-set and are termed the "new coefficients" (available
 182 in Table S2). The uncertainty formulations is designed to have an absolute error at low values and
 183 proportional error at larger values as will be expected as a result of uncertainties that are both
 184 instrumental and environmental.

185
 186 Unlike $K_d(490)^{NASA/ESA}$, $K_d(490)^{QAA}$ was initially developed 9 with one single set of coeffi-
 187 cients for all satellite sensors. To ensure that using a "sensor-specific" set of coefficients (found in
 188 Table S2) for each satellite wasn't resulting in a bias in $K_d(490)$ retrieval between different sensors,
 189 we tested the retrieval of $K_d(490)^{QAA}$ for each sensor using level-3 gridded R_{rs} from each sensor for
 190 the month of July 2020. The same method of retrieving the IOPs from R_{rs} using QAA and subse-
 191 quently computing K_d was used for each sensor. The idea was to assess how each sensor-pair would
 192 retrieve K_d with their own input data (R_{rs}), and if using the sensor-specific coefficients resulted in
 193 a different distribution between sensors-pairs than when using the same coefficients for all sensors
 194 (in this case the specific ones derived for MODIS-Aqua). Statistical metrics were computed for
 195 both cases "same coefficients" and "sensor-specific coefficients" and are found in the Supplementary
 196 (Table S3).

197 2.6 Net Primary Production (NPP) models

198 To evaluate the impact of the revised $K_d(490)^{QAA}$ algorithm, we implemented it into two commonly
 199 used, global NPP models. We chose to evaluate solely $K_d(490)^{QAA}$, as the new parametrization
 200 yields similar performance to $K_d(490)^{NASA/ESA}$ and is more adapted to a global ocean with both
 201 Case-1 and Case-2 waters. The first model is the Vertically Generalized Production Model (VGPM).
 202 The VGPM is a chlorophyll-based model that relies on chlorophyll a (Chl *a*) concentration, day

length, the maximum possible rate of primary production at a given location (derived from Sea Surface Temperature (SST)), and a light-dependent function [23].

The Carbon-based Productivity Model (CbPM) computes phytoplankton biomass from particulate back-scattering (b_{bp}) and estimates growth rate (μ) from the observed chlorophyll to carbon ratio [24] compared to the median mixed layer irradiance. The updated version (CbPMv2) is used here [4], which attenuates light spectrally throughout the water column.

There are notable differences regarding the input of $K_d(490)^{QAA}$ between these models and how it is used; in both, monthly gridded $K_d(490)_{NewCoeffs}^{QAA} / K_d(490)_{Original}^{QAA}$ computed using QAA-retrieved a and b_b from R_{rs} are used as inputs. In VGPM, $K_d(490)$ is converted into $K_d(PAR)$ using Morel's algorithm [7] for a layer of thickness $1/K_d(490) m$. In CbPMv2, $K_d(490)$ is used to compute a spectral $K_d(\lambda)$.

Monthly mapped level-3 ocean color climatology from MODIS-Aqua were downloaded from the NASA Ocean Biology Distributed Active Archive Center (OB.DAAC) [5] for the whole mission. Monthly mixed-layer depths for 2021 required as input in the CbPM model were calculated from the data-assimilative HYCOM model output (using a density threshold of $0.03 kg.m^{-3}$ criteria) and were downloaded from the Ocean Productivity webpage [6]. Monthly nitrate climatological profiles were downloaded from the World Ocean Atlas select [25] (WOAselect) and nitracline depths were defined as the depth at which nitrate concentration (NO_3) $> 0.3\mu M$ per [4]. Climatology of $K_d(490)_{NewCoeffs}^{QAA}$ and $K_d(490)_{Original}^{QAA}$ were computed using L3 R_{rs} data from NASA's OB.DAAC to use as inputs in the NPP models. The new coefficients chosen to compute $K_d(490)_{NewCoeffs}^{QAA}$ were the ones recomputed for MODIS-Aqua.

When performing the annual assessment, monthly data (for the whole 20-year climatology) were averaged for each pixel. We compare the models by performing a single modification; either we use $K_d(490)_{NewCoeffs}^{Rrs}$ or $K_d(490)_{Original}^{Rrs}$, all other inputs were kept exactly the same. When computing the average percent difference over a given month, the sum of the difference was divided by the number of pixels with existing NPP data either in the whole ocean (for the global comparison) or in regions with either low ($K_d(490) < 0.026 m^{-1}$) or high ($K_d(490) > 0.1 m^{-1}$) $K_d(490)$ (for the regional analysis). All results reported here were weighted to account for the latitudinal changes in the pixel area.

⁵<https://oceancolor.gsfc.nasa.gov/l3/order/>

⁶<http://sites.science.oregonstate.edu/ocean.productivity/index.php>

233 3 Results

234 3.1 $K_d(490)$ retrieval

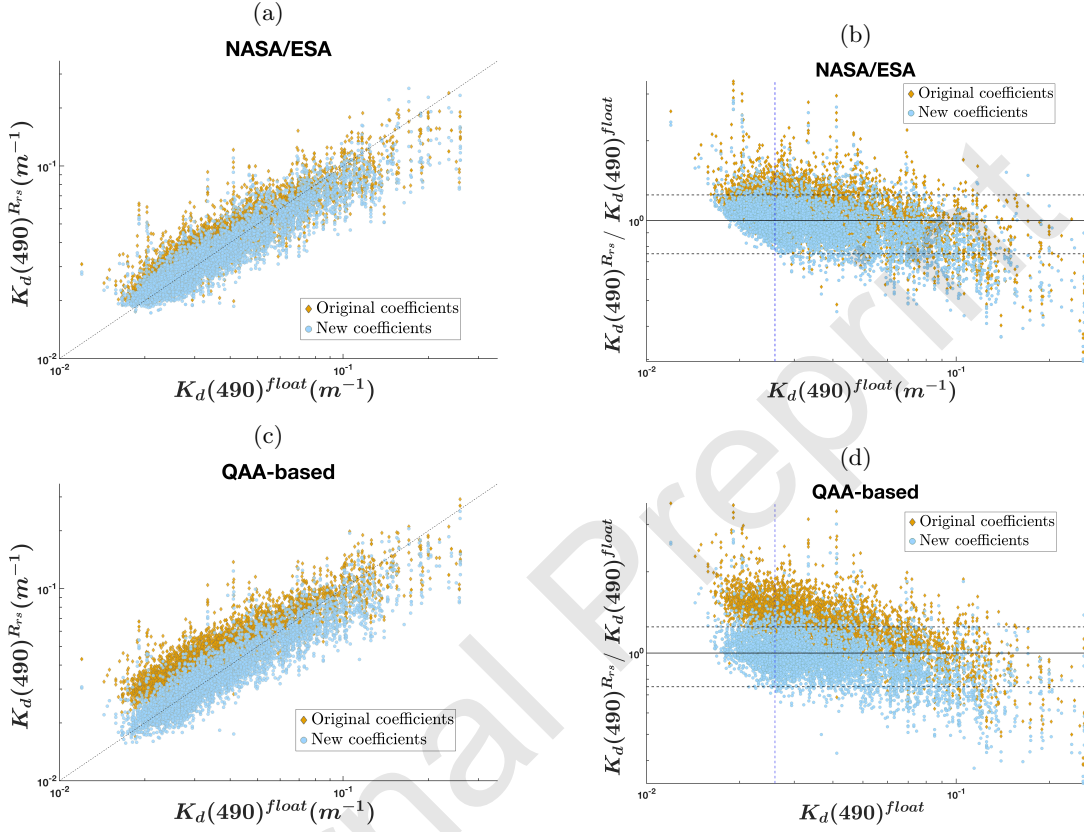


Figure 1: Comparison of $K_d^{R_{rs}}$ retrieval for the full match-up data-set (with all sensors grouped together) from two different algorithms with the newly computed vs. the original coefficients. (a) $K_d(490)_{NASA/ESA}^{R_{rs}}$ compared to $K_d(490)^{float}$. (b) Error ratio of $K_d(490)_{NASA/ESA}^{R_{rs}}$ to $K_d(490)^{float}$. (c) $K_d(490)_{QAA}^{R_{rs}}$ compared to $K_d(490)^{float}$. (d) Error ratio of $K_d(490)_{QAA}^{R_{rs}}$ to $K_d(490)^{float}$. New coefficients are listed in Table S2. The blue vertical line in (b) and (d) is 0.026, the minimum value of $K_d(490)$ in the NOMAD dataset.

235 Overall, for most satellite sensors the new coefficients resulted in an improvement for both algorithms
 236 ($K_d(490)_{NASA/ESA}^{R_{rs}}$ and $K_d(490)_{QAA}^{R_{rs}}$) with a bias closer to one and a lower ADP (Table 2), at the
 237 exception of OLCI-S3A for $K_d(490)_{NASA/ESA}^{R_{rs}}$.

238 $K_d(490)_{NewCoeffs}^{QAA}$ performs similarly to $K_d(490)_{NewCoeffs}^{NASA/ESA}$ for all measured statistical metrics
 239 and has a slope closer to one. The bias for the low values of $K_d(490) < 0.026 m^{-1}$ is no longer
 240 present although there appears to be a larger error ratio for some of the higher $K_d(490)$ values
 241 than with $K_d(490)_{Original}^{R_{rs}}$ (Figure 1). The number of match-ups with an error ratio (normalized
 242 difference between $K_d(490)^{R_{rs}}$ and $K_d(490)^{float}$) larger than $\pm 25\%$ when comparing the new vs.
 243 original coefficients decreased from 25% to 17% for $K_d(490)_{NASA/ESA}^{R_{rs}}$ and from 60% to 17% for

Table 2: Statistics for $K_d(490)^{Rrs}$ vs $K_d(490)^{float}$ for each of the six studied satellite sensors. For each sensor, a sub-sample was extracted at random to create an ensemble that has a proportion of data points from each biome consistent with the area covered by each biome. 100 ensembles (with random data points from each biome extracted every time) were added together to recreate a dataset representative (in proportion) of the ocean. Statistical metrics were computed on this proportional dataset. Bias is the median of the ratio between K_d^{Rrs} and K_d^{float} , Average Percent Difference (ADP) is as defined in [9], Root Mean Square Difference (RMSE) as defined in [8] and the slope between the log of the values is retrieved after performing a robust (bi-square weighting function) linear fit using the Matlab integrated function *fitlm*.

	NASA / ESA $K_d(490)$											
	MODIS-Terra		MODIS-Aqua		VIIRS-SNPP		VIIRS-JPSS		OLCI-S3A		OLCI-S3B	
Coefficients	Old	New	Old	New	Old	New	Old	New	Old	New	Old	New
Bias	1.17	1.00	1.18	1.00	1.08	0.98	1.07	0.99	1.02	0.93	1.17	1.00
ADP (%)	21.76	14.39	22.79	14.53	15.84	14.74	15.81	14.41	16.71	18.79	16.88	9.72
RMSE	0.01	0.01	0.01	0.01	0.01	0.01	0.01	0.01	0.01	0.02	0.01	0.01
r	0.87	0.87	0.88	0.88	0.87	0.87	0.91	0.91	0.74	0.74	0.95	0.97
Slope	0.95	1.00	0.95	0.99	0.98	1.01	0.98	1.00	0.98	1.01	0.96	1.00
	QAA-based $K_d(490)$											
	MODIS-Terra		MODIS-Aqua		VIIRS-SNPP		VIIRS-JPSS		OLCI-S3A		OLCI-S3B	
Coefficients	Old	New	Old	New	Old	New	Old	New	Old	New	Old	New
Bias	1.26	1.01	1.38	0.98	1.37	0.98	1.34	0.96	1.33	0.96	1.43	1.00
ADP (%)	29.67	14.77	38.55	16.03	37.82	14.06	34.88	14.27	33.47	14.17	38.90	12.59
RMSE	0.01	0.01	0.02	0.01	0.02	0.01	0.01	0.01	0.02	0.02	0.01	0.01
r	0.86	0.86	0.86	0.85	0.88	0.87	0.91	0.91	0.78	0.77	0.94	0.94
Slope	0.93	0.99	0.91	1.00	0.90	1.00	0.91	1.01	0.92	1.00	0.90	1.00

244 $K_d(490)^{QAA}$.

245 3.2 Independent validation

246 Since the float data-set was used in the derivation of the new coefficients there isn't complete
 247 independence between the two. We note, however, that the number of degrees of freedom in the
 248 data-set is much larger than the number of fitting coefficients computed, and hence they may be
 249 considered as, de-facto, independent.

250 In any case, the new coefficients were also validated in two additional ways. First, we used
 251 the same float data-set but assessed the performance of the QAA-based algorithm at a different
 252 wavelength, 412 nm. Since the coefficients were re-computed and fitted only using the 490 nm,
 253 $K_d(412)^{QAA}$ retrieval using those same coefficients is independent (as the $K_d(412)^{Rrs} / K_d(412)^{float}$
 254 match-ups were not used in the derivation of the new coefficient). There is a very significant
 255 improvement in retrieval for $K_d(412)$, with a smaller bias, a smaller ADP by 29%, a smaller RMSE,
 256 and a slope closer to 1 (Figure 2), with the small-value bias significantly better as only 28 % of
 257 the new coefficient values have an error ratio of $\pm 25\%$ now (compared to $\approx 70\%$ for the original
 258 coefficients).

259 The second way in which the new coefficients were independently assessed was by application to
 260 other data-sets of $R_{rs}-K_d(490)$ match-ups used to derive and assess K_d algorithms. The NOMAD,
 261 COASTLOOC, and synthetic IOCCG data span conditions from Case-1 to Case-2 waters and have
 262 a different statistical distribution than the float matchup database [1]. Performance in $K_d(490)$ -
 263 retrieval of those three databases decreases to some extent with the new coefficients: they result

264 in a higher ADP and RMSE (Figure 2) and a larger absolute bias. The new coefficients tend to
 265 underestimate $K_d(490)$. There are no significant differences in retrieval performance with the new
 266 coefficients when considering the full in-situ datasets or when selecting only data points correspond-
 267 ing to a Case-2 water type from the IOCCG, NOMAD and COASTLOOC datasets : in both cases
 268 the new coefficients perform less well. Note, however, that we have not weighted the performance
 269 metrics by the area of the oceans they are representing.

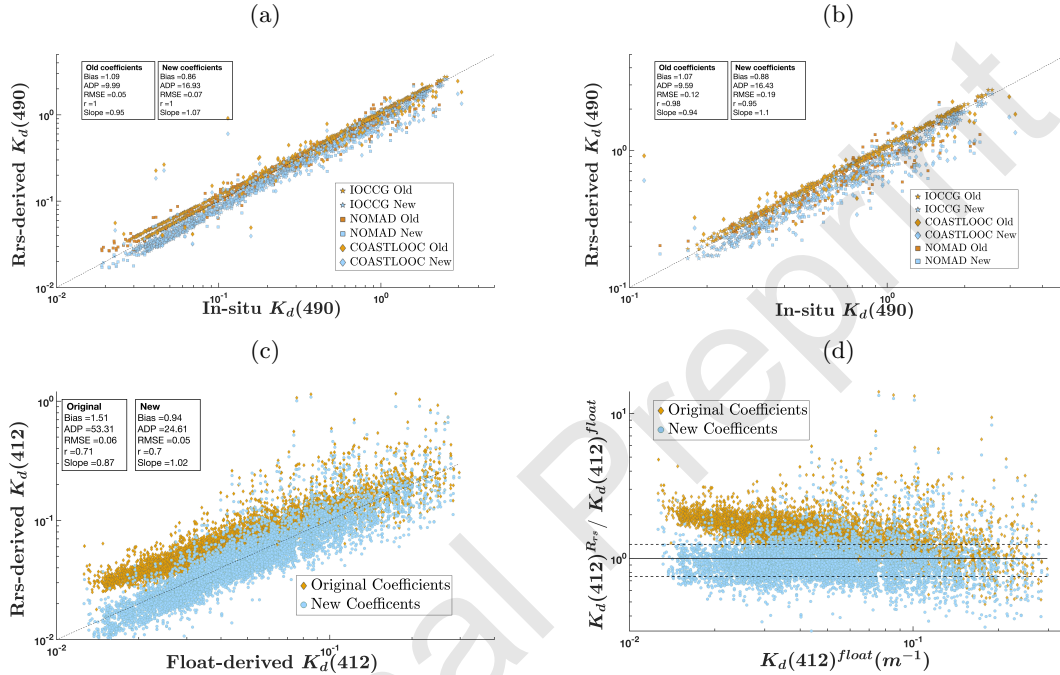


Figure 2: Comparisons between $K_d(\lambda)^{QAA}$ and $K_d(\lambda)^{inSitu}$ for independent databases not used in the computation of the new coefficients. (a) $K_d(490)^{QAA}$ versus $K_d(490)^{InSitu}$ with the original (Old) and the New coefficients. Shown here are NOMAD, COASTLOOC and the synthetic IOCCG database comparisons for the full data-sets. (b) $K_d(490)^{QAA}$ versus $K_d(490)^{InSitu}$ with the original (Old) and the New coefficients on Case-2 waters from the COASTLOOC and the synthetic IOCCG databases. (c) $Kd(412)^{QAA}$ versus $Kd(412)^{float}$ for the Original (orange) and the New (blue) coefficients. (d) Error ratio of $Kd(412)^{QAA} / Kd(412)^{float}$ for the Original (orange) and the New (blue) QAA coefficients.

270 3.3 Impact of new coefficients on Global Primary production quantifica- 271 tion

272 3.3.1 Annual comparison

273 Annual percentage differences between using $K_d(490)_{Original}^{QAA}$ or $K_d(490)_{NewCoeffs}^{QAA}$ (the difference
 274 between the two $K_d(490)^{QAA}$ will be referenced to as $K_d(490)_{Diff}^{QAA}$) as inputs in each of the two
 275 primary production models were computed; for VGPM (hereafter called ΔNPP_{VGPM}), the overall
 276 difference for the annual time series NPP shows a seasonal signal in areas with low $K_d(490)$ (Fig-
 277 ure 3), and to a lesser extent in areas with high $K_d(490)$. For the low $K_d(490)$ areas (defined as

278 $K_d(490) < 0.026 \text{ m}^{-1}$), we note a higher-than-average difference between original and new coeffi-
 279 cients, with a relative annual mean difference value of $\approx 79.2 \%$, and an absolute annual production
 280 difference of $7.88 \text{ Pg C.yr}^{-1}$. The percent difference is larger in the summer months for each hemi-
 281 sphere, with a maximum increase in late Spring and early Fall for the North Hemisphere. For the
 282 high $K_d(490)$ values (defined as $K_d(490) > 0.1 \text{ m}^{-1}$), the annual difference is significantly lower, with
 283 an average of $\approx -10\%$. The spatial pattern of difference in NPP retrieved from the VGPM model is
 284 correlated with the pattern of $K_d(490)_{Diff}^{QAA}$. The extent of ΔNPP_{VGPM} is similar to $K_d(490)_{Diff}^{QAA}$,
 285 with a smaller relative difference in the productive areas characterized by a large $K_d(490)$ and a
 286 large NPP_{VGPM} (such as the high latitudes of the northern hemisphere) and the highest difference
 287 in the areas with low $K_d(490)$ such as the subtropical gyres (Figure 3). When summing all data
 288 points within the climatology and weighting by each 1° pixel area, ΔNPP_{VGPM} is 35.53% , that is
 289 the use of $K_d(490)_{NewCoeffs}^{QAA}$ results a $\approx 35\%$ increase in the estimate of global primary production
 290 (increasing from $38.32 \text{ Pg C.yr}^{-1}$ to $53.86 \text{ Pg C.yr}^{-1}$).

291 The effect of changing $K_d(490)$ in CbPMv2 is different than of VGPM. ΔNPP_{CbPM} has an aver-
 292 age yearly difference in primary production of 38.66% ; production increased from $55.66 \text{ Pg C.yr}^{-1}$
 293 (using $K_d(490)_{Original}^{QAA}$) to $77.18 \text{ Pg C.yr}^{-1}$ (using $K_d(490)_{NewCoeffs}^{QAA}$). The maximum percentage
 294 difference is in the Southern Ocean and the North Atlantic (Figure 3). Regions of low $K_d(490)$ show
 295 a difference of 38.71% , an increase of $7.19 \text{ Pg C.yr}^{-1}$, consistent with the results from VGPM. In
 296 High $K_d(490)$ areas ($> 0.1 \text{ m}^{-1}$), ΔNPP_{CbPM} is also smaller on average (19.32%).

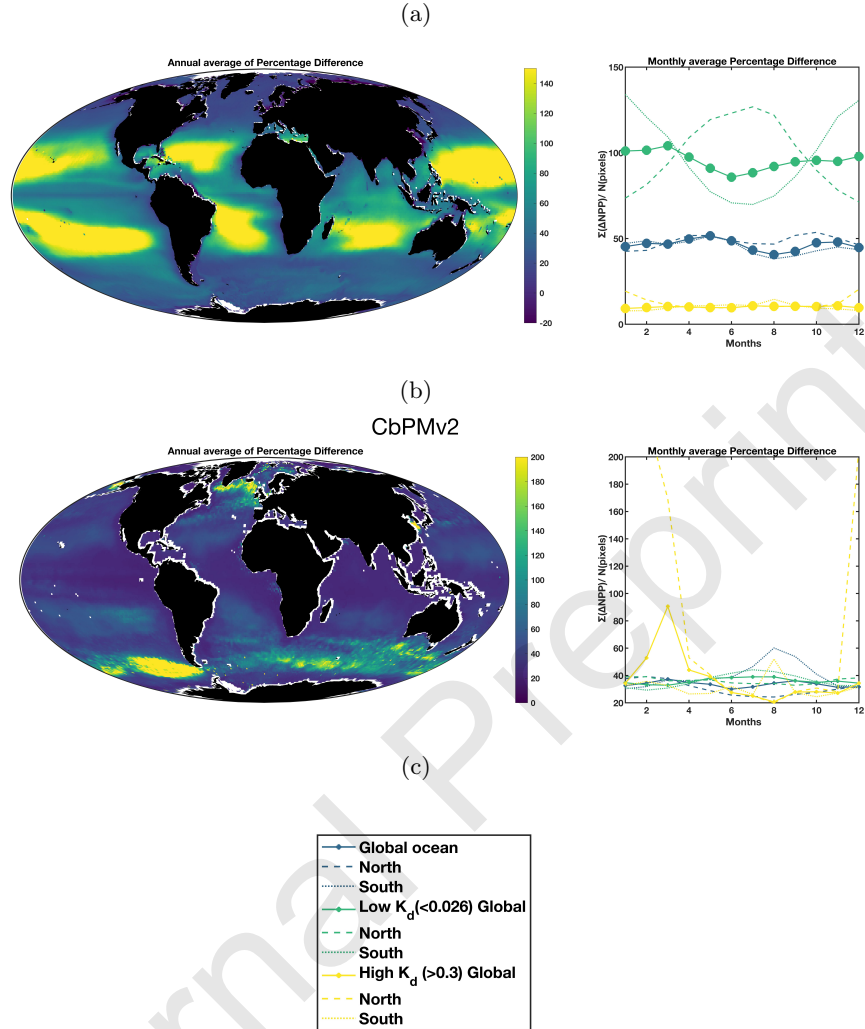


Figure 3: Difference in annual average NPP when using the original vs. the new coefficients as inputs in $K_d(490)^{QAA}$ using different Primary Production models. The left side is a map of the annual average percentage difference (%) and the right side is time series across months for regions with low $K_d(490)^{QAA} (< 0.026)$, high $K_d(490)^{QAA} (> 0.1)$ and for the overall region. Separation within each region is made for the North and South hemisphere to better represent seasonality. (a) Vertically Generalized Production Model (VGPM). (b) Carbon-based Productivity Model version 2 (CbPMv2). (c) Legend for the yearly climatology.

297 4 Discussion

298 In this work, we set as our goal to derive new coefficients for existing algorithms for $K_d(\lambda)$ so that
 299 they would be less biased *globally*. The use of weights in the fitting was designed so that the size of
 300 each biome and the number of match-ups within said biomes are taken into account. Additionally,
 301 we assumed a specific uncertainty for the fit (proportional to K_d except at low values) and minimized

302 a cost function based on absolute difference. This, of course, means that the fit is *different* from
 303 that which would be derived by weighing all match-ups equally, assuming the same uncertainty for
 304 all points and minimizing a cost-function based on root-mean-square.

305 A bias for small values of $K_d(490)$ had already been identified in previous studies, albeit with
 306 different cutoff values ($0.03 m^{-1}$ in [8] and $0.026 m^{-1}$ in [1]) but had not been addressed as it repre-
 307 sented a minimal proportion of the in-situ or simulated data-sets evaluated. However, a significant
 308 area of the ocean is characterized by clear waters with low $K_d(\lambda)$. Using the new coefficients we
 309 find the area where $K_d(490)_{NewCoeffs}^{QAA} < 0.026 m^{-1}$ during the climatology to represent 33% of the
 310 ocean (versus 0% with the original coefficients) and $K_d(490)_{NewCoeffs}^{NASA/ESA} < 0.026 m^{-1}$ represents 38%
 311 of the ocean (versus 24% for the original coefficients). Although primary production and carbon
 312 export are lower in these clear-water regions, the large areas they represent means that this bias is
 313 likely to have a significant impact on the quantification of physical and biological processes.

314 4.1 Improvement matching K_d for the BGC-Argo data-set

315 Using the new K_d coefficients resulted in significant improvement in the statistical metrics of match-
 316 ups between floats and satellites at the global scale, but the improvement varied depending on the al-
 317 gorithm and the sensor. $K_d(490)^{NASA/ESA}$ showed the smallest improvement, but it was still signifi-
 318 cant at the individual sensor level. The Austin and Petzold algorithm upon which $K_d(490)^{NASA/ESA}$
 319 is based was designed to work on clear Case-1 open-ocean waters so it is not surprising that it per-
 320 forms relatively well on the float data-set that is exclusively comprised of open-ocean measurements.
 321 The fact that there remains a bias (although of decreased amplitude) for low values when using
 322 the newly computed best-fit coefficients (Figure 1) is likely due to two factors: 1) The small values
 323 have a relatively low weight in the overall cost function, meaning that the cost function will try to
 324 minimize the bias for larger K_d values in priority (since they represent larger under-sampled ocean
 325 regions) and 2) the coefficients in the NASA/ESA algorithm are related to the blue/green band
 326 ratio of R_{rs} . The ratio might not be able to encompass the variability in K_d that is due to other
 327 parameters than the blue/green ratio (which is directly linked to the Chlorophyll *a* content of a
 328 water body [26]) such as the presence of high concentrations of Colored Dissolved Organic Matter
 329 (CDOM), Total Suspended Matter (TSM), and the effect of solar angle among others. Therefore,
 330 there would be limitations in the algorithm design itself, rather than in the coefficient recalculation
 331 per-se. Additionally, the blue/green spectral ratio follows an asymptotic shape, meaning that once
 332 it reaches a certain value of $K_d(490)$, the ratio will no longer be influenced by changes in $K_d(490)$
 333 [9]. The limitations of the NASA/ESA empirical algorithms are well documented and it is widely
 334 accepted to be only suitable for Case-1 relatively clear open ocean waters [8, 9, 27].

335 On the other hand, the semi-analytical algorithm generating $K_d(\lambda)^{QAA}$ was developed to work
 336 on a wide variety of waters and at all visible wavelengths, which means that the original range for
 337 which it was designed is much larger than for $K_d(490)^{NASA/ESA}$. However, no data used in either
 338 the computation of its original coefficients or the validation had values of $K_d(490)$ below $0.026 m^{-1}$
 339 [1, 9, 10] which likely caused the bias for small K_d values when the original coefficients were used.
 340 This bias was mostly resolved here, resulting in the number of match-ups with an error ratio greater

341 than 25% going from 60% to 17 %, which shows that using IOPs and solar angle might be a more
 342 robust way to retrieve $K_d(\lambda)$ than the link between $K_d(490)$ and a reflectance ratio associated with
 343 chlorophyll change when aiming to accurately retrieve the full range of variability found in nature.
 344 Although the small value bias appears to be resolved by the use of the new coefficients, the larger
 345 values in our data-set ($K_d(490) > 0.1 m^{-1}$) are more under-estimated than previously. Again, this
 346 appears to be due to the fact that they do have a lower weight in the final computation.
 347 The limited geographical area covered by the data in NOMAD (Gulf of Mexico, Eastern Coastal US,
 348 Pacific gyre and Mediterranean Sea) and COASTLOOC (Mediterranean Sea, Eastern and Coastal
 349 North Atlantic) means that they can almost be considered as a regional dataset. Given that we
 350 tried to recompute coefficients that work for the whole ocean, it is not surprising that a "regional"
 351 algorithm performs better than a global one in the specific region it was developed. The fact that
 352 there is little difference in the retrieval for the full datasets versus for the Case-2 water types using
 353 the new coefficients suggests that the modified algorithm is able to accurately retrieve Case-2 waters
 354 even though it wasn't derived with such data. However, we see a large variability in the new
 355 coefficients that were computed between sensors (Table S2). This leads to the conclusion that there
 356 may be too many coefficients tuned in this algorithm, resulting in several "solutions" when trying
 357 to determine the best coefficients that allow to compute $K_d(\lambda)$ from $a(\lambda)$ and $b_b(\lambda)$. Future work
 358 could explore if adjusting the number of coefficients and/or its explicit formalism could improve this
 359 algorithm .

360 Using sensor-specific coefficients versus one set of coefficients as inputs in $K_d(490)^{QAA}$ did result
 361 in slight differences between sensor-pairs (Table S3). Metrics indicate that using sensor-specific
 362 coefficients might result in slightly different retrieval of $K_d(490)$, which means that when using
 363 different satellite sensors to retrieve $K_d(\lambda)$, using the globally-derived coefficients (found in Table
 364 S2) might ensure a consistent retrieval between sensors.

365 4.2 Quantification of the bias in NPP

366 To assess the impact of the new algorithm, two different satellite-based primary production models
 367 were evaluated. The objective here was not to compare the performance of those models and
 368 assess which one was the closest to reality but to quantify how the change in $K_d(490)$ computation
 369 propagates to a change in primary production obtained from each individual model. VGPM's
 370 NPP, by design, is correlated with $K_d(490)$ [23] (Figure S4). Since the largest difference between
 371 $K_d(490)_{NewCoeffs}^{QAA}$ and $K_d(490)_{Original}^{QAA}$ occurs for small $K_d(490)$ values (Figure 1), the oligotrophic
 372 gyres show the highest ΔNPP_{VGPM} due to the underestimation of the euphotic depth. High
 373 $K_d(490)$ areas even show a small decrease in NPP ($-0.62 Pg C.yr^{-1}$), consistent with the pattern
 374 in $K_d(490)^{Diff}$.

375 Another notable feature in areas characterized by low $K_d(490)$, visible in the outputs of both
 376 VGPM and CbPMv2 , is the presence of a seasonal cycle in ΔNPP . Between summer (higher
 377 ΔNPP) and winter (lower ΔNPP), there are differences of $\approx 50\%$ for VGPM and $\approx 20\%$ for
 378 CbPMv2 (Figure 3).

379 The seasonal cycle in difference can also be attributed to the change in $K_d(490)$ in those olig-

380 otrophic waters, where $K_d(490)$ is strongly correlated with Chl a . In winter there is higher Chl
381 a (associated with a higher biomass of phytoplankton and/or photo-acclimation), resulting in a
382 larger $K_d(490)$. On the other hand, summer is characterized by stratified, nutrient-limited waters,
383 supporting a smaller amount of biomass of high-light adapted cells, effectively leading to a lower
384 $K_d(490)$ [28]. Since smaller $K_d(490)^{QAA}$ values have a larger bias than higher values, there are larger
385 ΔNPP_{VGPM} and ΔNPP_{CbPM} in the summer than in winter. This effect is not as pronounced for
386 the high $K_d(490)$ areas (defined here as $K_d(490) > 0.1m^{-1}$) for VGPM ($\approx -10\%$) since the bias was
387 smaller originally, and the reparametrization shows a slight overestimation of high $K_d(490)$ values,
388 which explains why there is a small decrease in yearly NPP in those regions.

389 CbPMv2 shows a very different spatial pattern than VGPM models, with ΔNPP_{CbPM} maximal
390 in regions associated with deep winter mixing. The design of the CbPMv2 model explains why it
391 behaves in a different manner: since NPP is integrated with depth until the bottom of the mixed
392 layer, the larger the layer, the larger the change in the amount of light (here our $\Delta K_d(490)$) will
393 have an effect (as it will propagate through the layer). It is important to note that those areas
394 with a very large mixed layer resulting in a large percentage change in NPP are in fact not very
395 productive, as they are limited by light availability. Therefore even if the percentage change is very
396 high (Figure 3), the magnitude of the effect of $\Delta K_d(490)$ is small in those areas (high $K_d(490)$ areas
397 show an overall increase of 1.70 to 2.03 $Pg C.yr^{-1}$ when changing the coefficients and the maximum
398 median monthly difference for the Southern hemisphere is in August and has an amplitude of 70%),
399 which explains why ΔNPP_{CbPM} (38.71%) is not much larger than ΔNPP_{VGPM} (35.53%), despite
400 having areas where annual average percentage differences reaching $\approx 150\%$ in the North Atlantic and
401 in the Southern Ocean (notably due to deep convective mixing in the North Atlantic Ocean).

402 Subtropical gyres represent 41% of the global ocean surface [29]. Numerous studies have at-
403 tempted to quantify NPP in the gyres either with in-situ measurements [29] or using models [30,
404 31] or both [32]. Estimates have historically ranged from 125 - 450 $mg C^{-2} d^{-1}$ [32]. Our findings
405 show the largest discrepancy between the new and original K_d coefficients for the VGPM model
406 happens in the subtropical gyres (characterized by very clear waters with small K_d s), and that it
407 has a non-negligible impact on the overall global primary production. Our results also indicate that
408 the subtropical gyres are responsible for a higher proportion of the global productivity of the ocean
409 and that their role has been previously underestimated. Updating the K_d coefficients and applying
410 them to the gyres' NPP estimates results in a net annual production change ranging from 7.19
411 $Pg C.yr^{-1}$ (CbPMv2) to 7.88 $Pg C.yr^{-1}$ (VGPM). In the context of a changing climate, with the
412 warming of the surface ocean and the associated decrease of vertical mixing, subtropical gyres are
413 expected to increase in area [33] and their NPP is expected to decrease [34]. It is thus important to
414 monitor how NPP changes in these areas with un-biased algorithms.

415 5 Summary

416 This study derived new coefficients for the computation of the spectral and planar diffuse atten-
417 uation of exiting algorithms, making them more consistent globally. Using these new coefficients
418 within commonly-used diffuse attenuation models (*NASA/ESA*, *QAA*) improves their performance

419 in optical water types ranging from Case-1 to Case-2. Previously computed attenuation coefficients
 420 were significantly over-estimated, resulting in an under-estimation of the depth to which light pene-
 421 trates in oligotrophic waters, particularly in the subtropical gyres. The effect of the newly-computed
 422 $K_d(490)$ on different NPP algorithms suggests that NPP was underestimated in the gyres by as much
 423 as 38% (CbPMv2 model) to 79.20% (CbPMv2 model). This results in a global bias in NPP. As ex-
 424 plained in [1], the underlying reason for the bias in attenuation was the lack of training data for
 425 algorithms from clear ocean regions and thus efforts should be made to continue to gather data rep-
 426 resentative of all areas of the oceans. BGC-Argo floats have been proven to be a very valuable tool
 427 for validation of global satellite products and here for their improvement and further deployments
 428 should be encouraged, as many regions of the globe are still under-sampled (e.g. the equatorial
 429 Pacific Ocean, [1]).

430 6 Supplementary

Table S1: Statistics for $K_d(490)^{Rrs}$ vs $K_d(490)^{float}$ for each of the six studied satellite sensors as well as for the full data-set. Bias is the median of the ratio between K_d^{Rrs} and K_d^{float} , Average Percent Difference (ADP) is as defined in [9], Root Mean Square Difference (RMSE) as defined in [8] and the slope and intercept value are retrieved after performing a robust (bisquare weighting function) linear fit using the Matlab integrated function *fitlm*.

		NASA / ESA $K_d(490)$											
		MODIS-Terra		MODIS-Aqua		VIIRS-SNPP		VIIRS-JPSS		OLCI-S3A		OLCI-S3B	
Coefficients		Old	New	Old	New	Old	New	Old	New	Old	New	Old	New
Bias		1.13	0.97	1.12	0.96	1.06	0.95	1.04	0.97	1.09	1.00	1.19	1.05
ADP (%)		20.53	16.74	19.76	16.52	17.33	16.69	17.10	16.12	18.47	16.46	22.08	16.76
RMSE		0.01	0.02	0.01	0.02	0.01	0.02	0.01	0.01	0.01	0.01	0.01	0.01
r		0.90	0.90	0.89	0.87	0.88	0.88	0.92	0.92	0.83	0.83	0.91	0.91
Slope		0.96	1.00	0.96	1.01	0.98	1.01	0.99	1.01	0.97	1.00	0.95	0.98
		QAA-based $K_d(490)$											
		MODIS-Terra		MODIS-Aqua		VIIRS-SNPP		VIIRS-JPSS		OLCI-S3A		OLCI-S3B	
Coefficients		Old	New	Old	New	Old	New	Old	New	Old	New	Old	New
Bias		1.27	1.01	1.37	0.99	1.36	0.98	1.34	0.96	1.33	1.00	1.39	1.00
ADP (%)		29.74	14.87	38.58	16.07	38.19	14.55	34.59	14.70	34.11	14.34	38.70	12.88
RMSE		0.01	0.01	0.02	0.01	0.02	0.01	0.02	0.01	0.02	0.02	0.01	0.01
r		0.87	0.87	0.86	0.85	0.86	0.86	0.91	0.90	0.75	0.75	0.94	0.94
Slope		0.93	0.99	0.91	1.00	0.90	1.01	0.91	1.01	0.92	1.00	0.90	1.00

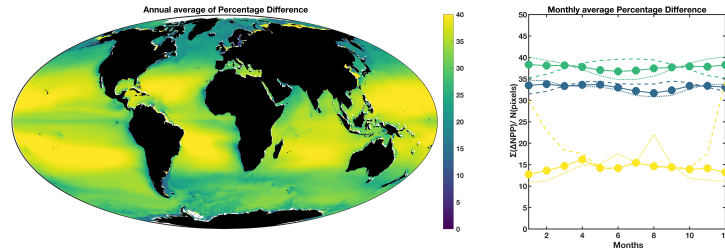


Figure 4: Difference in annual average $K_d(490)$ when using the original vs. the new coefficients as inputs.

Table S2: New coefficients that resulted in the smallest cost function for each of the two algorithms evaluated, and for each satellite sensor. If interested in code used to derive coefficients, see data availability section for link to GitHub repository. Original coefficients can be found in [1]

	$K_d(490)^{NASA/ESA}$					$K_d(\lambda)^{QAA}$			
	A0	A1	A2	A3	A4	A1	A2	A3	A4
MODIS-Terra	-0.9688	-2.1177	2.4232	-3.3654	-1.5287	0.7589	0.9845	0.5973	11.5902
MODIS-Aqua	-1.0437	-0.1871	-7.8081	15.5137	-12.8250	2.7842	0.0000	-3.4312	-35.2503
VIIRS-SNPP	-0.9331	-1.6787	1.0895	-2.1979	-1.0046	0.1502	-0.8199	1.2391	-3.1546
VIIRS-JPSS	-0.7693	-2.2239	1.7810	-2.4596	-1.0182	3.0194	0.0000	-2.4206	-35.2523
OLCI-S3A	-0.9365	-1.6523	0.9479	-1.5629	0.0889	0.3224	0.6513	0.7598	4.0967
OLCI-S3B	-0.9633	-0.7257	0.7890	-4.1177	0.0561	-0.2756	-1.5233	1.6874	-3.1597
Global	N/A	N/A	N/A	N/A	N/A	2.6188	1.2322	1.2351	38.8292

Table S3: Statistical metrics of the distribution of $K_d(490)^{QAA}$ derived from monthly level-3 R_{rs} data for July 2020 for each sensor-pair. In the top part are the metrics for when using a single set of coefficients derived for Modis-Aqua available in Table S2 and in the bottom part are the metrics when using the individual coefficients derived for each specific sensor available in Table S2

	Aqua vs. Terra	Aqua vs. Viirs	Aqua vs. OLCI-S3A	Aqua vs. OLCI-S3B	Viirs vs. Terra	Viirs vs. OLCI S3A	Viirs vs. OLCI-S3B	Terra vs. OLCI-S3A	Terra vs. OLCI-S3B	OLCI S3A vs. OLCI S3B
Using 1 set of Modis-Aqua coefficients.										
Bias	1.004	0.859	0.876	0.886	1.170	1.023	1.035	0.876	0.886	1.010
ADP	6.692	17.965	16.440	15.402	19.107	9.226	9.093	15.761	14.737	6.704
RMSE	0.143	0.522	0.582	0.581	0.120	0.428	0.223	0.225	0.214	0.136
Using the Individual sensor coefficients.										
Bias	1.063	1.039	0.866	0.981	1.037	0.833	0.956	0.813	0.929	1.141
ADP	12.761	9.437	17.446	13.419	9.685	21.523	12.194	26.254	9.737	18.197
RMSE	0.616	0.918	0.565	1.037	0.364	0.964	0.437	0.488	0.039	0.619

7 Author Contributions

"E. Boss and C. Begouen Demeaux conceived the idea. C. Begouen Demeaux performed the computations and analyzed the data. T. Westberry contributed to the interpretation of the NPP results and provided codes for the analysis. C. Begouen Demeaux wrote the first draft of the manuscript and all authors contributed to its revision."

8 Acknowledgments

The authors thank Marcel Babin for providing the COASTLOOC database. The authors thank all members of the BGC-Argo program without which this study would not have been possible. These data were collected and made freely available by the International Argo Program and the national programs that contribute to it (<https://argo.ucsd.edu>, <https://www.ocean-ops.org>). The Argo Program is part of the Global Ocean Observing System and data are accessible at <https://doi.org/10.17882/42182>. We thank Guillaume Bourdin and Nils Haentjens for coding help and advices.

444 Funding

445 This research was funded by NASA Ocean Biology and Biogeochemistry program grant number
446 80NSSC20M0203.

447 Conflicts of Interest

448 The authors declare that there is no conflict of interest regarding the publication of this article.

449 Data Availability

450 The matchup database between floats and Satellite-measured R_{rs} compiled by [1] was accessed
451 from the Zenodo open access platform using the following doi: [http://doi.org/10.5281/zenodo.](http://doi.org/10.5281/zenodo.7015427)
452 [7015427](http://doi.org/10.5281/zenodo.7015427). Level-3 satellite images were accessed from [https://oceancolor.gsfc.nasa.gov/l3/](https://oceancolor.gsfc.nasa.gov/l3/order/)
453 [order/](https://oceancolor.gsfc.nasa.gov/l3/order/) and MLD model outputs were accessed from [http://orca.science.oregonstate.edu/](http://orca.science.oregonstate.edu/2160.by.4320.monthly.hdf.mld030.hycom.php)
454 [2160.by.4320.monthly.hdf.mld030.hycom.php](http://orca.science.oregonstate.edu/2160.by.4320.monthly.hdf.mld030.hycom.php). Once peer-review process is complete, all codes
455 used to derive the new parametrization and to estimate NPP will be available on the Ocean Optics
456 Github page (<https://github.com/OceanOptics>).

457 References

- 458 [1] C. Begouen Demeaux and E. Boss, “Validation of Remote-Sensing Algorithms for Diffuse
459 Attenuation of Downward Irradiance Using BGC-Argo Floats,” en, *Remote Sensing*, vol. 14,
460 no. 18, p. 4500, 2022, ISSN: 2072-4292. DOI: [10.3390/rs14184500](https://doi.org/10.3390/rs14184500). [Online]. Available: [https://](https://www.mdpi.com/2072-4292/14/18/4500)
461 www.mdpi.com/2072-4292/14/18/4500 (visited on 11/02/2022).
- 462 [2] C. Mobley, *The Oceanic Optics Book*, en. International Ocean Colour Coordinating Group,
463 2022, Medium: 924pp. Publisher: International Ocean Colour Coordinating Group (IOCCG).
464 DOI: [10.25607/OBP-1710](https://doi.org/10.25607/OBP-1710). [Online]. Available: [https://repository.oceanbestpractices.](https://repository.oceanbestpractices.org/handle/11329/1853)
465 [org/handle/11329/1853](https://repository.oceanbestpractices.org/handle/11329/1853) (visited on 11/01/2022).
- 466 [3] P. R. Oke *et al.*, “Evaluation of a near-global eddy-resolving ocean model,” en, *Geoscientific*
467 *Model Development*, vol. 6, no. 3, pp. 591–615, 2013, ISSN: 1991-9603. DOI: [10.5194/gmd-](https://doi.org/10.5194/gmd-6-591-2013)
468 [6-591-2013](https://doi.org/10.5194/gmd-6-591-2013). [Online]. Available: <https://gmd.copernicus.org/articles/6/591/2013/>
469 (visited on 12/17/2022).
- 470 [4] T. Westberry, M. J. Behrenfeld, D. A. Siegel, and E. Boss, “Carbon-based primary produc-
471 tivity modeling with vertically resolved photoacclimation: CARBON-BASED PRODUCTION
472 MODEL,” en, *Global Biogeochemical Cycles*, vol. 22, no. 2, n/a–n/a, 2008, ISSN: 08866236.
473 DOI: [10.1029/2007GB003078](https://doi.org/10.1029/2007GB003078). [Online]. Available: [http://doi.wiley.com/10.1029/](http://doi.wiley.com/10.1029/2007GB003078)
474 [2007GB003078](http://doi.wiley.com/10.1029/2007GB003078) (visited on 11/02/2022).
- 475 [5] J. T. O. Kirk, *Light and Photosynthesis in Aquatic Ecosystems*, 3rd ed. Cambridge University
476 Press, 2010.

- 477 [6] R. W. Austin and T. J. Petzold, "The Determination of the Diffuse Attenuation Coefficient of
478 Sea Water Using the Coastal Zone Color Scanner," en, in *Oceanography from Space*, J. F. R.
479 Gower, Ed., Boston, MA: Springer US, 1981, pp. 239–256. DOI: [10.1007/978-1-4613-3315-](https://doi.org/10.1007/978-1-4613-3315-9_29)
480 [9_29](https://doi.org/10.1007/978-1-4613-3315-9_29). [Online]. Available: [http://link.springer.com/10.1007/978-1-4613-3315-](http://link.springer.com/10.1007/978-1-4613-3315-9_29)
481 [9_29](http://link.springer.com/10.1007/978-1-4613-3315-9_29) (visited on 11/02/2022).
- 482 [7] A. Morel, Y. Huot, B. Gentili, P. J. Werdell, S. B. Hooker, and B. A. Franz, "Examining
483 the consistency of products derived from various ocean color sensors in open ocean (Case 1)
484 waters in the perspective of a multi-sensor approach," en, *Remote Sensing of Environment*,
485 vol. 111, no. 1, pp. 69–88, 2007, ISSN: 00344257. DOI: [10.1016/j.rse.2007.03.012](https://doi.org/10.1016/j.rse.2007.03.012). [Online].
486 Available: <https://linkinghub.elsevier.com/retrieve/pii/S0034425707001307> (visited
487 on 11/02/2022).
- 488 [8] C. Jamet, H. Loisel, and D. Dessailly, "Retrieval of the spectral diffuse attenuation coefficient
489 in open and coastal ocean waters using a neural network inversion: RETRIEVAL OF DIFFUSE
490 ATTENUATION," en, *Journal of Geophysical Research: Oceans*, vol. 117, no. C10, n/a–n/a,
491 2012, ISSN: 01480227. DOI: [10.1029/2012JC008076](https://doi.org/10.1029/2012JC008076). [Online]. Available: [http://doi.wiley.](http://doi.wiley.com/10.1029/2012JC008076)
492 [com/10.1029/2012JC008076](http://doi.wiley.com/10.1029/2012JC008076) (visited on 11/02/2022).
- 493 [9] Z.-P. Lee, "Diffuse attenuation coefficient of downwelling irradiance: An evaluation of remote
494 sensing methods," en, *Journal of Geophysical Research*, vol. 110, no. C2, p. C02017, 2005,
495 ISSN: 0148-0227. DOI: [10.1029/2004JC002573](https://doi.org/10.1029/2004JC002573). [Online]. Available: [http://doi.wiley.com/](http://doi.wiley.com/10.1029/2004JC002573)
496 [10.1029/2004JC002573](http://doi.wiley.com/10.1029/2004JC002573) (visited on 11/02/2022).
- 497 [10] Z. Lee *et al.*, "Penetration of UV-visible solar radiation in the global oceans: Insights from
498 ocean color remote sensing: PENETRATION OF UV-VISIBLE SOLAR LIGHT," en, *Journal*
499 *of Geophysical Research: Oceans*, vol. 118, no. 9, pp. 4241–4255, 2013, ISSN: 21699275. DOI:
500 [10.1002/jgrc.20308](https://doi.org/10.1002/jgrc.20308). [Online]. Available: <http://doi.wiley.com/10.1002/jgrc.20308>
501 (visited on 11/02/2022).
- 502 [11] X. Xing, E. Boss, J. Zhang, and F. Chai, "Evaluation of Ocean Color Remote Sensing Al-
503 gorithms for Diffuse Attenuation Coefficients and Optical Depths with Data Collected on
504 BGC-Argo Floats," en, *Remote Sensing*, vol. 12, no. 15, p. 2367, 2020, ISSN: 2072-4292. DOI:
505 [10.3390/rs12152367](https://doi.org/10.3390/rs12152367). [Online]. Available: <https://www.mdpi.com/2072-4292/12/15/2367>
506 (visited on 11/02/2022).
- 507 [12] Z. Lee, "Penetration of solar radiation in the upper ocean: A numerical model for oceanic and
508 coastal waters," en, *Journal of Geophysical Research*, vol. 110, no. C9, p. C09019, 2005, ISSN:
509 0148-0227. DOI: [10.1029/2004JC002780](https://doi.org/10.1029/2004JC002780). [Online]. Available: [http://doi.wiley.com/10.](http://doi.wiley.com/10.1029/2004JC002780)
510 [1029/2004JC002780](http://doi.wiley.com/10.1029/2004JC002780) (visited on 01/24/2023).
- 511 [13] X. Xing and E. Boss, "Chlorophyll-Based Model to Estimate Underwater Photosynthetically
512 Available Radiation for Modeling, *In-Situ* , and Remote-Sensing Applications," en, *Geophys-*
513 *ical Research Letters*, vol. 48, no. 7, Apr. 2021, ISSN: 0094-8276, 1944-8007. DOI: [10.1029/](https://doi.org/10.1029/2020GL092189)
514 [2020GL092189](https://doi.org/10.1029/2020GL092189). [Online]. Available: [https://onlinelibrary.wiley.com/doi/10.1029/](https://onlinelibrary.wiley.com/doi/10.1029/2020GL092189)
515 [2020GL092189](https://onlinelibrary.wiley.com/doi/10.1029/2020GL092189) (visited on 02/03/2023).

- 516 [14] S. W. Bailey and P. J. Werdell, “A multi-sensor approach for the on-orbit validation of ocean
517 color satellite data products,” en, *Remote Sensing of Environment*, vol. 102, no. 1-2, pp. 12–
518 23, 2006, ISSN: 00344257. DOI: [10.1016/j.rse.2006.01.015](https://doi.org/10.1016/j.rse.2006.01.015). [Online]. Available: [https://
519 //linkinghub.elsevier.com/retrieve/pii/S0034425706000472](https://linkinghub.elsevier.com/retrieve/pii/S0034425706000472) (visited on 12/12/2022).
- 520 [15] E. Organelli *et al.*, “A Novel Near-Real-Time Quality-Control Procedure for Radiometric Pro-
521 files Measured by Bio-Argo Floats: Protocols and Performances,” en, *Journal of Atmospheric
522 and Oceanic Technology*, vol. 33, no. 5, pp. 937–951, 2016, ISSN: 0739-0572, 1520-0426. DOI:
523 [10.1175/JTECH-D-15-0193.1](https://doi.org/10.1175/JTECH-D-15-0193.1). [Online]. Available: [https://journals.ametsoc.org/view/
524 journals/atot/33/5/jtech-d-15-0193_1.xml](https://journals.ametsoc.org/view/journals/atot/33/5/jtech-d-15-0193_1.xml) (visited on 11/02/2022).
- 525 [16] A. R. Fay and G. A. McKinley, “Global open-ocean biomes: Mean and temporal variability,”
526 en, *Earth System Science Data*, vol. 6, no. 2, pp. 273–284, 2014, ISSN: 1866-3516. DOI: [10.
527 5194/essd-6-273-2014](https://doi.org/10.5194/essd-6-273-2014). [Online]. Available: [https://essd.copernicus.org/articles/6/
528 273/2014/](https://essd.copernicus.org/articles/6/273/2014/) (visited on 12/19/2022).
- 529 [17] Z.-P. Lee, Ed., *Remote sensing of inherent optical properties: Fundamentals, tests of algorithms,
530 and applications*. 2006.
- 531 [18] Z. Lee, K. L. Carder, and R. A. Arnone, “Deriving inherent optical properties from water
532 color: A multiband quasi-analytical algorithm for optically deep waters,” en, *Applied Optics*,
533 vol. 41, no. 27, p. 5755, Sep. 2002, ISSN: 0003-6935, 1539-4522. DOI: [10.1364/AO.41.005755](https://doi.org/10.1364/AO.41.005755).
534 [Online]. Available: <https://opg.optica.org/abstract.cfm?URI=ao-41-27-5755> (visited
535 on 01/31/2023).
- 536 [19] R. M. Pope and E. S. Fry, “Absorption spectrum (380–700 nm) of pure water II Integrating
537 cavity measurements,” en, *Applied Optics*, vol. 36, no. 33, p. 8710, Nov. 1997, ISSN: 0003-6935,
538 1539-4522. DOI: [10.1364/AO.36.008710](https://doi.org/10.1364/AO.36.008710). [Online]. Available: [https://opg.optica.org/
539 abstract.cfm?URI=ao-36-33-8710](https://opg.optica.org/abstract.cfm?URI=ao-36-33-8710) (visited on 02/09/2023).
- 540 [20] X. Zhang, L. Hu, and M.-X. He, “Scattering by pure seawater: Effect of salinity,” en, *Optics
541 Express*, vol. 17, no. 7, p. 5698, Mar. 2009, ISSN: 1094-4087. DOI: [10.1364/OE.17.005698](https://doi.org/10.1364/OE.17.005698).
542 [Online]. Available: <https://opg.optica.org/oe/abstract.cfm?uri=oe-17-7-5698>
543 (visited on 02/09/2023).
- 544 [21] P. J. Werdell and S. W. Bailey, “An improved in-situ bio-optical data set for ocean color algo-
545 rithm development and satellite data product validation,” en, *Remote Sensing of Environment*,
546 vol. 98, no. 1, pp. 122–140, 2005, ISSN: 00344257. DOI: [10.1016/j.rse.2005.07.001](https://doi.org/10.1016/j.rse.2005.07.001). [Online].
547 Available: <https://linkinghub.elsevier.com/retrieve/pii/S0034425705002208> (visited
548 on 12/19/2022).
- 549 [22] T. Zhang and F. Fell, “An empirical algorithm for determining the diffuse attenuation co-
550 efficient K_d in clear and turbid waters from spectral remote sensing reflectance: K_d in
551 clear and turbid waters,” en, *Limnology and Oceanography: Methods*, vol. 5, no. 12, pp. 457–
552 462, Dec. 2007, ISSN: 15415856. DOI: [10.4319/lom.2007.5.457](https://doi.org/10.4319/lom.2007.5.457). [Online]. Available: [http:
553 //doi.wiley.com/10.4319/lom.2007.5.457](http://doi.wiley.com/10.4319/lom.2007.5.457) (visited on 02/09/2023).

- 554 [23] M. J. Behrenfeld and P. G. Falkowski, "Photosynthetic rates derived from satellite-based
555 chlorophyll concentration," en, *Limnology and Oceanography*, vol. 42, no. 1, pp. 1–20, 1997,
556 ISSN: 00243590. DOI: [10.4319/10.1997.42.1.0001](https://doi.org/10.4319/10.1997.42.1.0001), [Online]. Available: <http://doi.wiley.com/10.4319/10.1997.42.1.0001> (visited on 12/02/2022).
- 558 [24] M. J. Behrenfeld, E. Boss, D. A. Siegel, and D. M. Shea, "Carbon-based ocean productivity
559 and phytoplankton physiology from space: PHYTOPLANKTON GROWTH RATES AND
560 OCEAN PRODUCTIVITY," en, *Global Biogeochemical Cycles*, vol. 19, no. 1, 2005, ISSN:
561 08866236. DOI: [10.1029/2004GB002299](https://doi.org/10.1029/2004GB002299), [Online]. Available: <http://doi.wiley.com/10.1029/2004GB002299> (visited on 12/02/2022).
- 563 [25] T. P. Boyer *et al.*, *World ocean atlas 2018*, 2018. [Online]. Available: <https://www.ncei.noaa.gov/archive/accession/NCEI-WOA18>.
- 565 [26] M. S. Salama and W. Verhoef, "Two-stream remote sensing model for water quality mapping:
566 2SeaColor," en, *Remote Sensing of Environment*, vol. 157, pp. 111–122, 2015, ISSN: 00344257.
567 DOI: [10.1016/j.rse.2014.07.022](https://doi.org/10.1016/j.rse.2014.07.022), [Online]. Available: <https://linkinghub.elsevier.com/retrieve/pii/S0034425714002715> (visited on 12/17/2022).
- 569 [27] K. Alikas, S. Kratzer, A. Reinart, T. Kauer, and B. Paavel, "Robust remote sensing algo-
570 rithms to derive the diffuse attenuation coefficient for lakes and coastal waters: Algorithm
571 for diffuse attenuation coefficient," en, *Limnology and Oceanography: Methods*, vol. 13, no. 8,
572 pp. 402–415, 2015, ISSN: 15415856. DOI: [10.1002/lom3.10033](https://doi.org/10.1002/lom3.10033), [Online]. Available: <https://onlinelibrary.wiley.com/doi/10.1002/lom3.10033> (visited on 12/17/2022).
- 574 [28] M. Stramska and P. Aniskiewicz, "Recent Large Scale Environmental Changes in the Mediter-
575 ranean Sea and Their Potential Impacts on Posidonia Oceanica," en, *Remote Sensing*, vol. 11,
576 no. 2, p. 110, 2019, ISSN: 2072-4292. DOI: [10.3390/rs11020110](https://doi.org/10.3390/rs11020110), [Online]. Available: <http://www.mdpi.com/2072-4292/11/2/110> (visited on 12/17/2022).
- 578 [29] J. Marra and K. Heinemann, "Primary production in the North Pacific Central Gyre: Some
579 new measurements based on c14," en, *Deep-Sea Research*, 1986.
- 580 [30] W. Balch, R. Evans, J. Brown, G. Feldman, C. McClain, and W. Esaias, "The remote sensing
581 of ocean primary productivity: Use of a new data compilation to test satellite algorithms,"
582 en, *Journal of Geophysical Research*, vol. 97, no. C2, p. 2279, 1992, ISSN: 0148-0227. DOI:
583 [10.1029/91JC02843](https://doi.org/10.1029/91JC02843), [Online]. Available: <http://doi.wiley.com/10.1029/91JC02843>
584 (visited on 12/17/2022).
- 585 [31] P. Lobanova, G. H. Tilstone, I. Bashmachnikov, and V. Brotas, "Accuracy Assessment of
586 Primary Production Models with and without Photoinhibition Using Ocean-Colour Climate
587 Change Initiative Data in the North East Atlantic Ocean," en, *Remote Sensing*, vol. 10, no. 7,
588 p. 1116, 2018, ISSN: 2072-4292. DOI: [10.3390/rs10071116](https://doi.org/10.3390/rs10071116), [Online]. Available: <http://www.mdpi.com/2072-4292/10/7/1116> (visited on 12/19/2022).
- 589

- 590 [32] A. Regaudie-de-Gioux *et al.*, “Multi-model remote sensing assessment of primary production
591 in the subtropical gyres,” en, *Journal of Marine Systems*, vol. 196, pp. 97–106, Aug. 2019,
592 ISSN: 09247963. DOI: [10.1016/j.jmarsys.2019.03.007](https://doi.org/10.1016/j.jmarsys.2019.03.007). [Online]. Available: [https://
593 linkinghub.elsevier.com/retrieve/pii/S0924796318303385](https://linkinghub.elsevier.com/retrieve/pii/S0924796318303385) (visited on 01/03/2023).
- 594 [33] A. J. Irwin and M. J. Oliver, “Are ocean deserts getting larger?” en, *Geophysical Research
595 Letters*, vol. 36, no. 18, p. L18609, Sep. 2009, ISSN: 0094-8276. DOI: [10.1029/2009GL039883](https://doi.org/10.1029/2009GL039883).
596 [Online]. Available: <http://doi.wiley.com/10.1029/2009GL039883> (visited on 01/16/2023).
- 597 [34] S. R. Signorini, B. A. Franz, and C. R. McClain, “Chlorophyll variability in the oligotrophic
598 gyres: Mechanisms, seasonality and trends,” en, *Frontiers in Marine Science*, vol. 2, 2015,
599 ISSN: 2296-7745. DOI: [10.3389/fmars.2015.00001](https://doi.org/10.3389/fmars.2015.00001). [Online]. Available: [http://journal.
frontiersin.org/Article/10.3389/fmars.2015.00001/abstract](http://journal.
600 frontiersin.org/Article/10.3389/fmars.2015.00001/abstract) (visited on 12/20/2022).